Journal of Atmospheric and Solar-Terrestrial Physics 69 (2007) 1587–1598

Journal of ATMOSPHERIC AND SOLAR-TERRESTRIAL PHYSICS

www.elsevier.com/locate/jastp

Modeling the responses of the middle latitude ionosphere to solar flares

Huijun Le[a,b], Libo Liu[a,*], Bin Chen[a], Jiuhou Lei[d], Xinan Yue[a,b,c], Weixing Wan[a]

[a] *Institute of Geology and Geophysics, Chinese Academy of Sciences, Beijing 100029, P. R. China*
[b] *Graduate School of the Chinese Academy of Science, Beijing 100049, P. R. China*
[c] *Wuhan Institute of Physics and Mathematics, Chinese Academy of Sciences, Wuhan 430071, P. R. China*
[d] *High Altitude Observatory, National Center for Atmospheric Research, Boulder, CO 80301, USA*

Received 24 October 2006; received in revised form 15 June 2007; accepted 15 June 2007
Available online 22 June 2007

Abstract

In this paper, we investigate the solar flare effects of the ionosphere at middle latitude with a one-dimensional ionosphere theoretical model. The measurements of solar irradiance from the SOHO/Solar EUV Monitor (SEM) and GOES satellites have been used to construct a simple time-dependent solar flare spectrum model, which serves as the irradiance spectrum during solar flares. The model calculations show that the ionospheric responses to solar flares are largely related to the solar zenith angle. During the daytime most of the relative increases in electron density occur at an altitude lower than 300 km, with a peak at about 115 km, whereas around sunrise and sunset the strongest ionospheric responses occur at much higher altitudes (e.g. 210 km for a summer flare). The ionospheric responses to flares in equinox and winter show an obvious asymmetry to local midday with a relative increase in total electron content (TEC) in the morning larger than that in the afternoon. The flare-induced TEC enhancement increases slowly around sunrise and reaches a peak at about 60 min after the flare onset.

Keywords: Mid-latitude ionosphere; Modeling and forecasting; Flares

1. Introduction

The solar flare is a sudden eruption solar phenomenon, associated with significant enhancements in extreme ultraviolet (EUV) and X-ray radiations. These transient enhancements of solar irradiance would greatly affect the state of the ionosphere. The solar flares and their immediate consequences take place in periods of minutes to hours. Since the 1960s, the responses of the ionosphere to solar flares have been studied continuously with various methods, such as the Faraday rotation measurement, incoherent scatter radar (ISR), and global positioning system (GPS). For example, Donnelly (1967, 1969) reported the sudden frequency deviation (SFD) during flare events. Garriott et al. (1967, 1969) observed a sudden increase in total electron content (TEC) recorded by the VHF signals from the ATS-1 satellite. Thome and Wagner (1971) analyzed the height distribution of increases in electron density Ne during the May 1967 flares on the basis of ISR observations. Mendillo and Evans (1974) analyzed the global

*Corresponding author. Tel.: +86 10 62007427.
E-mail address: liul@mail.iggcas.ac.cn (L. Liu).

1364-6826/$ - see front matter
doi:10.1016/j.jastp.2007.06.005

solar flare observations by using 17 stations in North America, Europe, and Africa for the first time and addressed that the enhancement of TEC at low latitude was higher than that at high latitude. Wan et al. (2005) analyzed the sudden increase of total electron content (SITEC) during the July 14, 2000 flare by the GPS data and found that both the flare-induced TEC variation rate and the TEC enhancement are proportional to the flare radiation I_f and inversely proportional to the Chapman function ch(χ). Recently, global views of solar flare effects of the ionosphere by using the GPS network observations have been achieved (e.g. Afraimovich, 2000; Leonovich et al., 2002; Liu et al., 2004; Tsurutani et al., 2005; Zhang et al., 2002; Zhang and Xiao, 2005). Afraimovich (2000) developed a novel technique to detect global ionospheric effects of solar flares, and effects of two powerful flares of the ionosphere were studied as examples. Leonovich et al. (2002) proposed a new method to estimate the contribution to the enhancements of TEC at different altitudes for the July 14, 2000 flare, and found that 25% of the TEC increments come from altitudes above 300 km. Zhang et al. (2002) reported that the TEC enhancement becomes smaller when the solar zenith angle (SZA) is larger. Liu et al. (2004) suggested that TEC is a suitable tool to monitor the overall variations of flare radiations, while the rate of change of TEC (rTEC) is capable of detecting sudden changes in the flare radiations. Tsurutani et al. (2005) reported persistence in TEC for several hours on the October 28, 2003 flare and found strong center-to-limb effects in the solar flare EUV spectra by comparing the October 28, 2003 flare event with the November 4, 2003 event. By using the GPS data from 114 GPS stations of the International GPS Service for Geodynamics (IGS), Zhang and Xiao (2005) analyzed the morphological features of the TEC variations in the sunlit hemisphere during the solar flare on October 28, 2003. Furthermore, Chen et al. (2005) statistically analyzed the SITEC caused by intense solar flares during 1996–2003 and found a negative relationship between the TEC enhancements and the distance between the Earth and Sun (seasonal effect), and also a negative relationship between the amplitude of SITEC and the duration of the flares.

The above investigations are mostly concentrated on case studies with various data sets (e.g. ISR, GPS measurements). A comparison of the modeled and observed flares effects of the ionosphere is essential to verify the ability of ionospheric models and enrich our knowledge on the production and loss mechanisms of the ionosphere. However, modeling studies on the ionospheric responses to the flare are still seldom found in literature, partly due to the absence of the observed information on the full spectrum of solar radiations during the course of solar flares. In order to overcome this difficulty, Warren et al. (1998, 2001) introduced a new approach for modeling solar EUV irradiance variation. Based on the method of Warren et al. (1998, 2001) and the observations of the Bastille Day flare, Meier et al. (2002) estimated the flare EUV spectral irradiance enhancement and predicted the ionospheric response to the flare radiation. Furthermore, using a time-dependent EUV spectrum (Mariska et al., 1989), Huba et al. (2005) presented the first global simulation study on the ionospheric effects associated with the enhanced EUV irradiance of the Bastille Day flare. Both Meier et al. (2002) and Huba et al. (2005) focused on the modeling of the special flare event.

In this paper, we investigate the ionosphere effects of the flares which occurred at different local times (LT) and different seasons with a one-dimensional mid-latitude ionosphere theoretical model (Lei et al., 2004a, b). First of all, we simulate the ionospheric responses to the flare event on October 28, 2003. A time-dependent solar flare spectrum on this day has been constructed based on observations of the SOHO Solar EUV Monitor (SEM) EUV and the GOES X-ray. The modeling results are compared with the GPS-TEC observations. Then we focus on the ionospheric response to flares under different local times and seasons.

2. Ionospheric model and the solar flare EUV spectrum

A one-dimensional theoretical model for the mid-latitude ionosphere used in this study has been developed by Lei et al. (2004a, b). Using this model, equations of mass continuity and momentum for O^+ are solved. Ion densities of NO^+, O_2^+, and N_2^+ are calculated under the assumption of photochemical equilibrium. Neutral compositions are taken from the NRLMSISE-00 model (Picone et al., 2002), and the NO density is obtained from an empirical model developed by Titheridge (1997). In this paper, we expand the height of the upper boundary from 600 to 1000 km for better calculation of the TEC value. The reader is referred to Lei et al. (2004b) for a detailed description on the model.

The EUVAC model (Richards et al., 1994) empirically provides the solar EUV flux at 37 wavelength bins, covering the range of 50−1050 Å, but does not include the X-ray wavelength bins. Richards et al. (2006) present a new high-resolution version of the EUVAC model (HEUVAC) to improve the spectrum resolution. The HEUVAC model has constant wavelength bins over the range 0–1050 Å with any resolution desired. In this study, the solar spectra (5−1045 Å) are separated into 208 wavelength bins with 5 Å resolution. In this paper, the HEUVAC model is used to provide the solar radiation fluxes for our ionospheric model. However, during a solar flare, the solar X-ray and EUV fluxes vary significantly, especially for shorter wavelengths. To obtain a more realistic flare spectrum profile, the SOHO/SEM 260−340 Å data with 15 s time resolution and the GOES X-ray (1−8 Å) data with 1 min resolution are used to serve as reference fluxes during a flare. The values of the radiation 1 h before solar flare onset are set as the background level, and the radiation during the flare course is obtained by multiplying the background level by a time-varied coefficient $\alpha_i(t)$, where t is the lapsed time after the onset of flare, and i indicates the ith wavelength bin ($i = 1, 2, \ldots, 208$). The time-varied coefficients of 300–305 Å, α_{60}, and 5–10 Å, α_1, are directly taken from the SOHO/SEM 260–340 Å data and the GOES X-ray 1−8 Å data. The coefficients of other bins are obtained as follows:

$$\alpha_i(t) = \begin{cases} \alpha_1(t)A_i/A_1 & \text{for } i \leqslant 10, \\ \alpha_{60}(t)A_i/A_{60} & \text{for } i > 10. \end{cases} \quad (1)$$

Here A_i ($i = 1, 2, \ldots, 208$), the ratio of the flare irradiation at the peak of a flare to the pre-flare irradiation at 1 h before the flare, is obtained according to Woods and Eparvier (2006). The SOHO/SEM integrated (26–34 nm) EUV photon flux and the GOES X-ray flux during the October 28, 2003 flare are plotted in Fig. 1. The corresponding coefficients of α_{60} and α_1 are also shown in Fig. 1. We constructed the time-dependent solar spectrum of the October 28, 2003 flare according to Eq. (1) for the following model calculations.

The data from GOES satellite show that the October 28, 2003 flare is the fourth most intense (X17.2) in the NOAA records, with the solar radiation flux of 1–8 Å X-rays increased by a factor of more than 20. However, this flare is not a special one with regard to the time evolutions of X-ray and EUV flux. To clarify this point, we select randomly three flare events (July 14, 2000, X5.7; April 6, 2001, X5.6; and June 11, 2003, X1.6) to make comparison with the October 28, 2003 flare. According to the GOES X-ray 1−8 Å data, the rise times (from the background level to the peak) during the four flare events on July 14, 2000, April 6, 2001, June 11, 2003, and October 28, 2003 are about 21, 11, 13, and 12 min, respectively; the decay times (from peak to 1/2 peak) are about 19, 10, 13, and 14 min, respectively; so the ratios of the rise time to the decay time of the 1–8 Å X-ray flux are 0.904, 0.909, 1.0, and 1.17, respectively. According to the SOHO/SEM EUV 260–340 Å data, the rise times during the four flare events are 22, 11, 9, and 8 min, respectively; the decay times are 24, 15, 13, and 13 min, respectively; so the ratios of the rise time to the decay time of the 260–340 Å flux are 0.916, 0.733, 0.692, and 0.615, respectively. One can infer that there are no obvious differences between the October 28 flare and the other three flares regarding the time evolutions of X-ray and EUV flux. The larger solar flare presents a better opportunity to study the response of the ionosphere to the variation of solar radiation flux because the ionospheric response could be greater. So the data of 1–8 Å X-rays and 260–340 Å EUV flux during the October 28 flare are adopted as reference spectrum to construct a simple time-dependent solar flare spectrum.

The primary photoionization for O^+, O_2^+, and N_2^+ can be calculated when the absorption and photoionization cross sections for the temperatures and densities of neutral atomic oxygen (O), molecular oxygen (O_2), and nitrogen (N_2) are known, together with the above solar radiation flux. Besides the above three kinds of ions, the photoionization of molecule NO is also calculated in the model (Lei et al., 2004b), which could improve the simulation for lower altitudes. The solar radiation ionizes the neural components O, O_2, and N_2 and primary free photoelectrons are released. Some of these primary photoelectrons have enough energy to induce secondary ionization and/or even several times of ionization. In the model, we adopt the approach of Titheridge (1996) to calculate the secondary ionization rate.

3. Simulation results and discussion

First we test the ability of the model to simulate the ionospheric response to the October 28, 2003

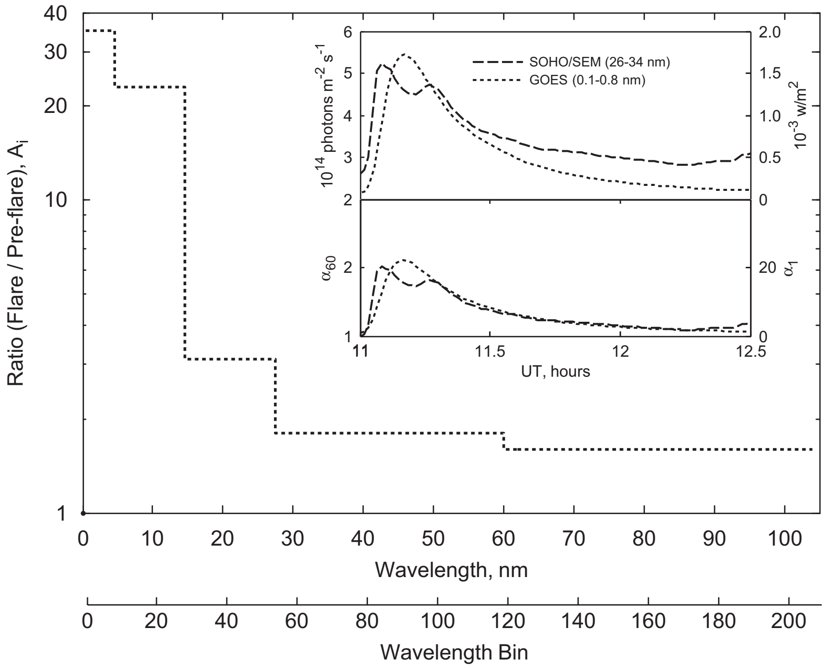

Fig. 1. The ratio of the flare irradiation at the time of flare peak to the pre-flare irradiation at 1 h before flare, A_i ($i = 1, 2\ldots, 208$), which is obtained according to Woods and Eparvier (2006). The SOHO/SEM integrated (26–34 nm) EUV photon flux and the GOES X-ray energy flux during the flare on October 28, 2003 are also shown in the top panel (inset). The time-varied coefficients of 300−305 Å, α_{60} (dashed line), and 5–10 Å, α_1 (dotted line), are also plotted in the bottom panel (inset).

flare event. The calculations are conducted at a location of geographic latitude 48°N and longitude 0°E. The following geophysical parameters are adopted: DOY (day of year) = 301, $F10.7 = 254$, $F10.7A = 138.7$, 3 h geomagnetic index AP = (15 39 22 39 12 27 18 27). We simulate the flares at different LT and DOY. The geophysical conditions are set to be the same as those on October 28, 2003.

It should be noted that during the flare the time step Δt of the ionosphere model is taken as 60 s to be consistent with the 1-min time resolution of GOES X-ray data, and at other times it is set as 300 s. In each simulation, we perform two runs: one with the normal spectrum throughout the process and the other with the time-dependent flare spectra.

3.1. Case study: October 28, 2003 flare

In Fig. 2, the simulated results are plotted together with the observations derived from three GPS stations at Innsbruck of Austria (HFLK, 47.3°N, 11.4°E), Bregenz of Austria (PFAN, 47.5°N, 9.8°E), and Karlsrube of Germany (KARL, 49.0°N, 8.4°E). The vertical TEC data are derived from the ninth satellite (#9) by assuming an ionospheric spherical shell at an altitude of 650 km (Tsurutani et al., 2005). These three stations are chosen because their geographical locations are close to the simulated location (48°N, 0°E). We define the enhancement of TEC, $\Delta TEC = TEC_f – TEC_0$. TEC_f is the TEC on October 28, 2003 and TEC_0, the background TEC, is obtained by fitting the curve of TEC before and after a solar flare. For the simulated results, TEC_f stands for the TEC with flare; TEC_0 for the TEC without flare. As illustrated in Fig. 2b, there are double peaks in the SOHO/SEM EUV. The first and larger peak occurs at about 1105 UT and the second peak at 1116 UT. The observed ΔTEC increases rapidly from about 1100 to 1105 UT, and then increases slower from about 1105 to 1118 UT (Fig. 2a). A peak in ΔTEC with about 16 TECU is reached at 1118 UT. Similar to the observations, the simulated ΔTEC also increases rapidly from 1100 to 1105 UT, and increases slower and then reaches the peak value of about 12 TECU at 1118 UT. One can find that the evolutions of the modeled and observed ΔTEC are in good agreement, except for some minor difference in the amplitude of ΔTEC.

Good agreements between observations and simulations indicate that the model used in this

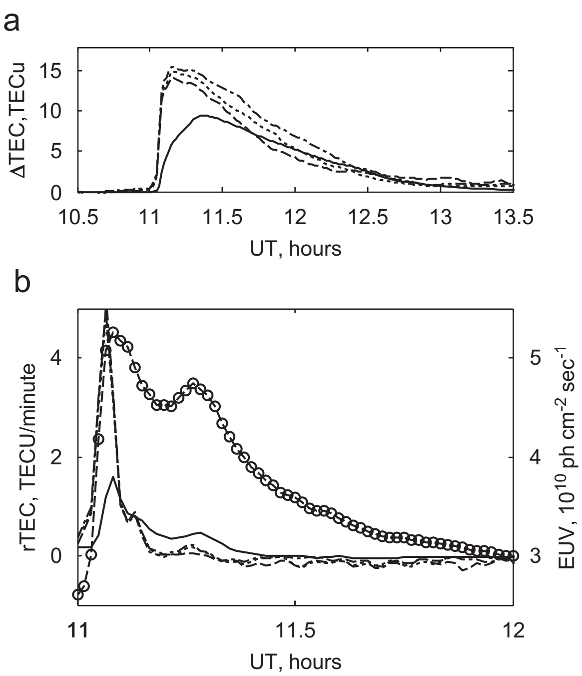

Fig. 2. (a) The comparison of the modeled ΔTEC with observed ΔTEC from the GPS data. (b) The comparison of the modeled rTEC with observed rTEC from the GPS data. The solid lines stand for simulation; the dotted lines for HFLK (11.4°E, 47.3°N); the dash–dotted lines for PFAN (9.8°E, 47.5°); and the dashed lines for KARL (8.4°E, 49.0°N). In addition, the dashed circle line with *y*-axis on the right side of graph (b) represents the EUV intensity of the SOHU/SEM 260–340 Å on October 28, 2003. 1 TECU = 10^{16} el/m^2.

study is feasible for the modeling of the ionospheric response to the flare. As shown in Fig. 2b, both the observed and modeled rTEC have two peaks corresponding to the double peaks of solar EUV. It suggests that the rTEC is more suitable to monitor the sudden changes in solar radiations during flares, which supports the conclusion of Liu et al. (2004). However, there are also some differences between the GPS data and the modeled result. The observed TEC increases more rapidly during the flare. We note that there are some uncertainties in this simulation. First we only obtain the 260–340 Å EUV and the 1–8 Å X-ray, while other wavelength bins are obtained by scaling these reference spectrums with Eq. (1). Furthermore, there are uncertainties in the neutral gas densities calculated from the MSIS model because the MSIS model does not include the flares affect on the thermosphere.

3.2. The characteristics from the simulations

To investigate the seasonal effects of flare-induced enhancements in electron density, we take days 81, 171, 261, and 351 as spring, summer, autumn, and winter, respectively. The ionospheric responses to a flare in four seasons were simulated by using the ionospheric model at different local times. In the following, the lapsed time after flare onset will be frequently used, which is abbreviated as TAFO. Due to the high similarity between the simulated results on day 81 and on day 261, we only split a year into three seasons and choose the simulated results on days 81, 171, and 351 to represent the ionospheric responses to a flare in equinox, summer, and winter solstices, respectively.

3.2.1. The electron density variations

Ne_f and Ne_0 denote the values of Ne with a flare and without a flare, respectively. Define the absolute increase in Ne, $\Delta Ne = Ne_f–Ne_0$, and the relative increase in Ne, $r\Delta Ne = \Delta Ne/Ne_0$. In the paper, we focus on the relative change of electron density rΔNe and not on the absolute increase ΔNe, because the relative change reflects the ionospheric response to solar flare more exactly than the absolute increase. Fig. 3a–c shows the flare-induced relative increase rΔNe at different local times in three seasons. The left panels of Fig. 3 show the results around sunrise; the right panels of Fig. 3 show the

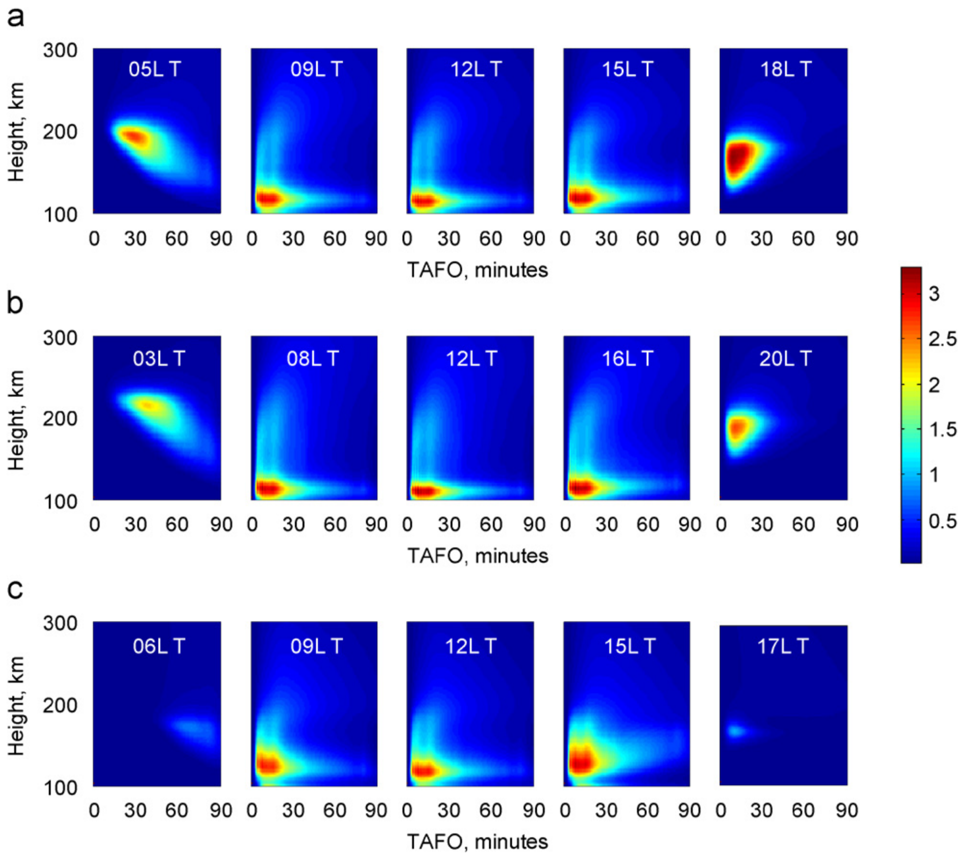

Fig. 3. The profiles of the simulated rΔNe in (a) equinox (DOY = 81), (b) summer (DOY = 171), and (c) winter (DOY = 351). The local time on each panel stands for the onset time of the flare.

results around sunset; and the middle three panels correspond to the results during the daytime. From Fig. 3 we find that during the daytime most of rΔNe occurs in the region below 300 km, which agrees with the finding of Thome and Wagner (1971), and the largest rΔNe occurs in the E-region (at an altitude about 115 km) with a factor of more than 3. During a flare, much more significant increase of X-ray and short-wavelength EUV radiation, which are mainly absorbed in the E-region, should be responsible for the largest rΔNe in the E regions. The height of the largest rΔNe almost remains at 110–120 km during the whole course of the flare in three seasons, which is due to the dominant photochemical processes at the low ionosphere (Rishbeth and Garriott, 1969). Fig. 3 also illustrates that the simulated results around sunrise and sunset are quite different from those during the daytime. During the daytime, the response of the E region ionosphere at low altitudes to the flare is stronger than that at high altitudes, with a peak at about 115 km altitude; however, around sunrise and sunset (e.g. 05 and 18 LT, 03 and 20 LT, and 06 and 17 LT on days 81, 171, and 351, respectively), because of a higher $1/e$ penetration depth due to the larger SZA, the flare-induced radiation enhancements are mainly absorbed at higher altitudes, which causes the stronger responses at high altitudes than at low altitudes, with a peak at about 150–200 km. Moreover, the ionospheric responses to a flare have no significant differences during the daytime.

To clearly illustrate the altitude distribution of the ionospheric response to a flare, we plot the height profiles of the daytime rΔNe in three seasons in Fig. 4. As seen from Fig. 4, there is the largest rΔNe in the E-region at about 115 km, as mentioned above, and also a second smaller peak in the F-region at about 180 km. Most of the F region photoionization comes from solar radiations at the middle bands, 260–796 Å, whereas radiation at longer and shorter wavelengths contributes more at lower attitudes (Hargreaves, 1992). During a flare, the largest enhancements in ionizing radiation occur at short wavelengths lower than 10 nm

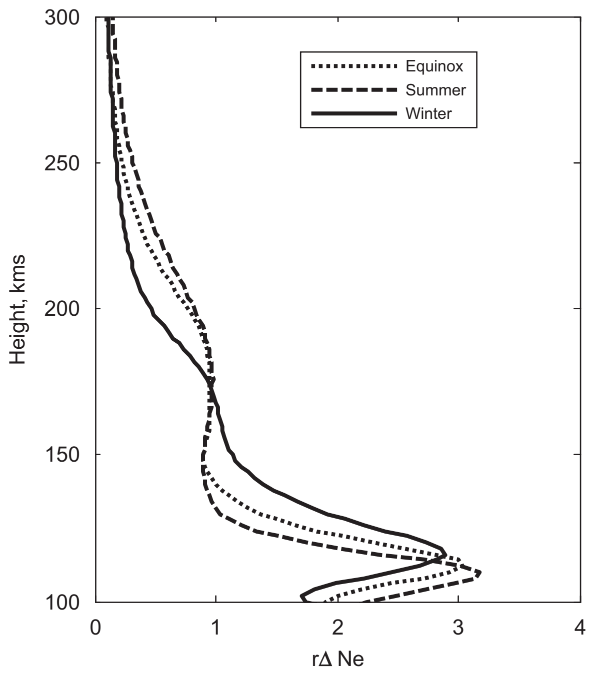

Fig. 4. The height profiles of the simulated rΔNe in the daytime for three seasons: equinox, summer, and winter, respectively. The data are simulated results of 12 LT and the time is at TAFO = 10 min.

that are absorbed in the E-region, so the largest rΔNe lies in the E-region. The high similarity of the three lines in Fig. 4 also indicates that during the daytime there are only small differences in the ionospheric response with season.

The peak rΔNe is defined as the largest value of rΔNe among all altitudes during the whole period of a flare. We plot the local time dependence of the height of peak rΔNe (abbreviated as Hpr) in Fig. 5a. Fig. 5b illustrates the corresponding variation of peak rΔNe and Fig. 5c for the corresponding SZA variation. As seen from Fig. 5a, the shape of the variation of Hpr with local time looks like "U"; that is, Hpr around sunrise and sunset is much higher than that during the daytime. Taking the results of equinox, for example, Hpr drops gradually from about 210 to 116 km during the time from sunrise to morning (04–08 LT), stays at about 116 km during the daytime (08–16 LT), and uplifts from 116 to 190 km during the time from 16 to 18 LT. Fig. 5a also shows that during the daytime Hpr is lowest (about 110 km) in summer and highest (about 120 km) in winter. Comparing Fig. 5a with c, one can infer that the variation of SZA is likely to be the main reason for the seasonal discrepancies and the local time variations of Hpr. The SZA is smallest in summer and largest in winter, which would directly cause Hpr to be the smallest in summer and largest in winter. The larger SZA around sunrise and sunset cause more flare radiation to be absorbed by the ionosphere at higher altitudes and then cause larger Hpr around sunrise and sunset than during the daytime. The variations of the peak rΔNe with local time in Fig. 5b show that the peak rΔNe is largest at 1 or 2 h after sunrise (e.g. 06, 04, and 07 LT in equinox, summer, and winter, respectively), and reaches nearly a factor of 4. This result may be because the background electron density at that time is lowest. We also find that during the daytime there are only very small changes in the peak rΔNe with local time.

In Fig. 6, the simulated results in equinox are selected to illustrate the evolutions of the rΔNe at different altitudes around sunrise, daytime, and sunset, respectively. The results in other seasons (not shown) are similar to those in equinox. As seen from Fig. 6, the ionospheric responses depend on altitude and local time significantly. The results during daytime and sunset are similar, which is that the rΔNe at altitudes below 200 km increases rapidly with the peak at TAFO ≈ 6–8 min and then decreases rapidly, whereas the rΔNe at altitudes above 200 km increases slower than that at altitudes below 200 km, reaching the peak at TAFO ≈ 20 min, and then also decreases slower than altitudes below 200 km. The domination of the photochemical processes, large neutral gas densities, and large X-ray and short-wavelength EUV enhancements was mainly absorbed at low altitudes. These combined factors lead to a rapid increase in the rΔNe in this region. Molecular ions such as NO^+ and O_2^+, the dominant ion at low altitudes, have a much rapid dissociative recombination rate. This also causes a rapid decrease in rΔNe in this region. At high altitudes, the domination of the transport processes other than photochemical processes, less neutral gas densities, and less middle band EUV enhancements mainly absorbed in the F-region (Hargreaves, 1992) cause a slower increase in rΔNe in this region. In the F-region (above 200 km), the loss process of the dominant ion O^+ mainly by the ion–atom interchange reaction is much slow compared with the dissociative recombination of molecular ions, which cause a slower decrease in the rΔNe in this region. As shown in the left panel of Fig. 6, around sunrise the ionospheric response is faster and larger at higher altitudes: obvious

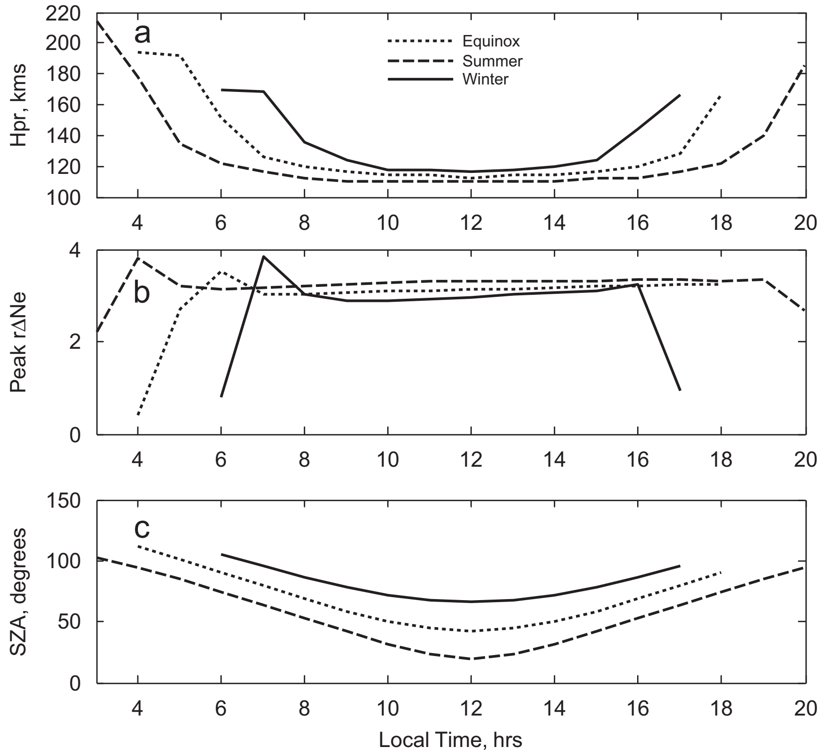

Fig. 5. (a) The height of peak rΔNe during the flare at different local times; (b) the corresponding peak rΔNe during the flare; and (c) the corresponding solar zenith angles in equinox, summer, and winter, respectively. This peak rΔNe is the largest value of rΔNe among all altitudes during the whole period of flare.

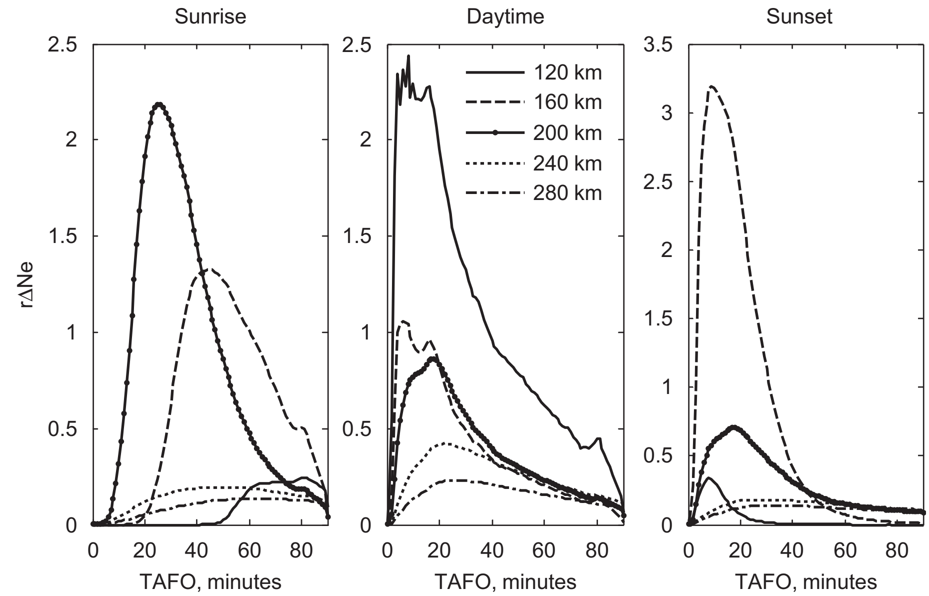

Fig. 6. The time evolution of the relative change in Ne, rΔNe, at altitudes of 120, 160, 200, 240, and 280 km, when a flare occurs around sunrise (05 LT, SZA = 101.1°), daytime (12 LT, SZA = 42.7°), and sunset (18 LT, SZA = 90.1°) in equinox.

increases occur at TAFO ≈ 20 min, with a peak rΔNe of about 1.3 at 160 km, and at TAFO ≈ 40 min, with a peak rΔNe of about 0.25 at 120 km, whereas electron densities begin to increase at TAFO ≈ 5 min, with the peak rΔNe of about 2.3 at 200 km. Around sunrise, during the initial time of flare due to a very large SZA, the EUV and X-ray could not penetrate deep enough to low altitudes because of the absorption along the long ray path of radiation by dense neutral atmosphere. Therefore, an obvious and rapid increase of electron density at low altitudes does not exist. However, with increase in time the corresponding SZA decreases, which makes it possible for EUV and X-ray to reach a lower altitude gradually and causes the ionospheric altitudes of 160 and 120 km to begin to present flare response at TAFO ≈ 20 and 40 min. However, the rapid increase in electron density at low altitudes as occurs in the daytime will not occur (as shown in the left panel of Fig. 6 that rΔNe at 120 and 160 km reaches its peak at TAFO ≈ 70 and 45 min) because both X-ray and EUV radiations decrease from TAFO ≈ 20 min (see Fig. 1). The greater flare response around sunrise at high altitudes should be due to the low electron density compared with those at daytime and sunset.

3.2.2. The TEC variations

The evolutions of the relative change in TEC, rΔTEC, around sunrise, daytime, and sunset are shown in Fig. 7. The relative change in TEC is defined by the ratio $(TEC_f–TEC_0)/TEC_0$, where TEC_f stands for the TEC with a flare and TEC_0 for the no flare case. The results in other seasons are similar to those in equinox, and are therefore not plotted here. As illustrated in Fig. 7, during daytime and near sunset, the rΔTEC increases rapidly, with a peak at TAFO ≈ 18 min (slightly delayed from the flare peaks at TAFO ≈ 5 and 16 min), then decays gradually with time. The speed of the increase of *r*ΔTEC is 3–4 times fast as that of decrease. However, during sunrise the rΔTEC increases slowly and reaches the peak at TAFO ≈ 60 min and then decays slowly. Around sunrise, due to a very large SZA, short EUV and X-ray could only mainly be absorbed by the atmosphere at high altitudes, which causes a small TEC increase. With the time increasing and SZA becoming smaller, the short EUV and X-ray could gradually reach lower altitudes and product larger photo-ionizations, which causes TEC to increase until some time before solar radiations return to the background

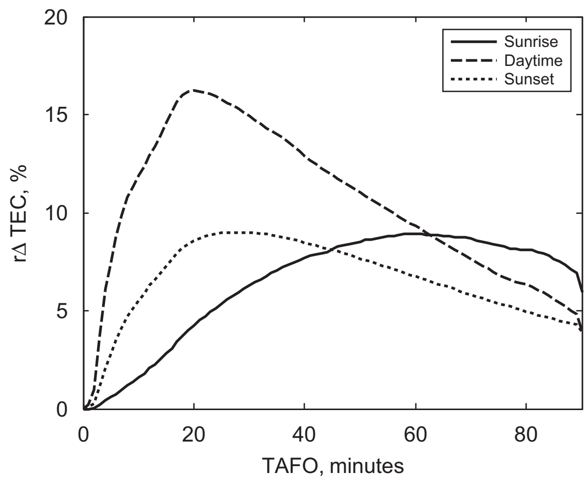

Fig. 7. The time evolution of the relative change in TEC, rΔTEC, when a flare occurs around sunrise (05 LT, SZA = 101.1°), daytime (12 LT, SZA = 42.7°), and sunset (18 LT, SZA = 90.1°) in equinox.

level. Similar results are illustrated in the left panel of Fig. 6. During the first 20 min there is no obvious increase at altitudes below 200 km. There is a small increase at TAFO ≈ 20 min for the altitude of 160 km and at TAFO ≈ 50 min for the altitude of 120 km. The rΔTEC at 120, 160, and 200 km reaches the maximum at TAFO ≈ 70, 45, and 25 min, respectively. At the time of the flare onset, SZA is larger around sunrise than around sunset because the sunrise LT is 7 h before noon and the sunset LT is only 6 h after noon. The larger SZA causes smaller TEC increase at the initial time of a flare. Furthermore, the SZA around sunrise decreases gradually with time, whereas the SZA around sunset increases gradually with time. The decreasing of SZA with time causes TEC to increase slowly for a long time. These two factors might be the reason for the difference between sunrise and sunset TEC behaviors in Fig. 7.

Fig. 8 shows the dependence of peak rΔTEC on the local time in three seasons. This peak rΔTEC is the largest value of the simulated rΔTEC during the whole period of the flare. The dotted lines indicate the variation of SZA. We also plotted the dependence of the corresponding background TEC, TEC_0, on the local time in three seasons in the right panels of Fig. 8. The simulated results show that, in all seasons, both in the morning and afternoon, the absolute increase in TEC (TEC_f–TEC_0, not plotted) is related to the SZA. The smaller the SZA, the more the TEC enhancement.

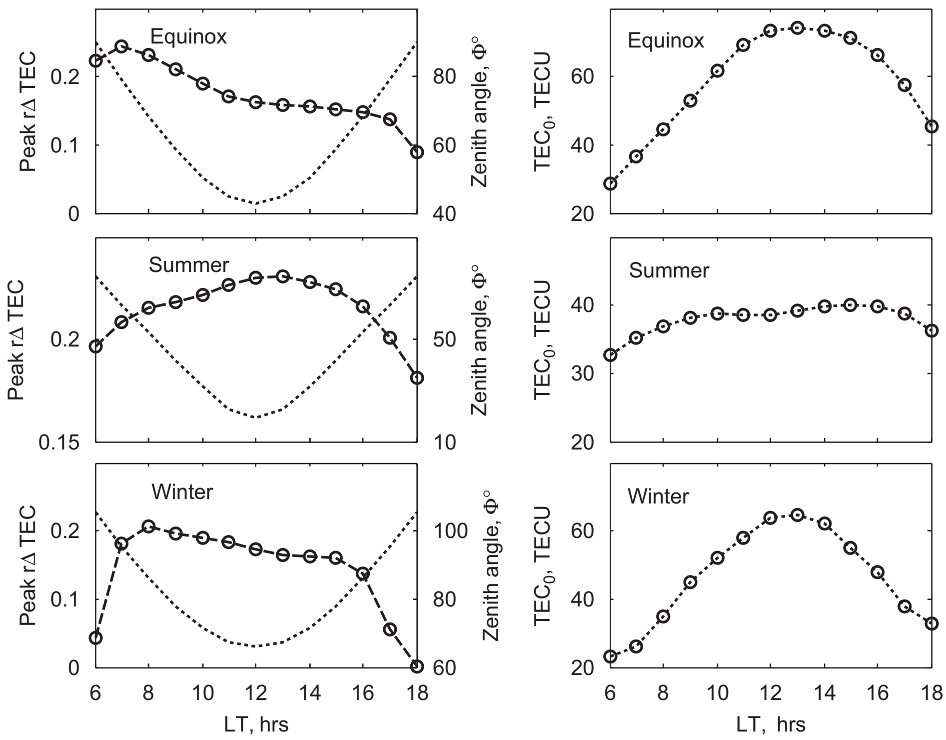

Fig. 8. Left panels: the dependence of peak rΔTEC on local time in three seasons (the dashed circle lines); the dotted lines indicate the variation of solar zenith angle. Right panels: the dependence of the corresponding background TEC, TEC_0, on local time in three seasons. This peak rΔTEC is the largest simulated values of rΔTEC during the whole period of flare.

Their correlation is in accord with Chapman ionospheric theory (Rishbeth and Garriott, 1969). It is because that the smaller the SZA, the more solar the radiations absorbed at low altitudes which would cause larger electron production rates. From Fig. 8 we can see that, in all seasons, the peak rΔTEC in the afternoon has an obvious negative correlation with SZA. For the peak rΔTEC in the morning, in summer it is smaller when the SZA is larger, whereas in equinox and winter it is larger when the SZA is larger. Fig. 8 shows that there is a smaller background TEC (TEC_0) in the morning in equinox and winter, and it leads to the larger relative increase in TEC (rΔTEC). An obvious feature of the local time asymmetry to local noon occurs during a flare in equinox and winter, with larger rΔTEC in the morning than in the afternoon as shown in Fig. 8. Similar asymmetrical features were also reported by Zhang and Xiao (2000, 2002). In addition, we also find that in equinox and winter the largest rΔTEC occurs at some time early morning (e.g. 07 LT in equinox and 08 LT in winter), which is also due to the much lower background TEC in the early morning. However, in summer it occurs at about 12 LT because the asymmetry of the background TEC in summer is small, not as obvious as in other seasons.

4. Concluding remarks

In this study, we have presented the ionospheric effects associated with the solar flare that occurred in different seasons and local times. We find that the ionospheric response to a flare is mainly related to solar zenith angle. The main results can be summarized as follows:

1. Most of the Ne enhancements responding to a flare occur in the E and low F regions (below 300 km). During the daytime, rΔNe at low altitudes is much larger than that at high altitudes, with a peak at about 115 km and a second smaller peak at about 180 km. Much more significant increase of X-ray and short-wavelength EUV radiation should be responsible for the larger rΔNe in the E regions. In the daytime, there are only small changes in the ionospheric response with season.

2. Around sunrise and sunset, due to the larger SZA, the strongest ionospheric response to the flare lies at much higher altitudes, as high as 190, 210, and 170 km in equinox, summer, and winter, respectively. During the daytime, the height of the strongest ionospheric response is lowest (about 110 km) in summer and highest (about 120 km) in winter due to the smallest SZA in summer and the largest SZA in winter.
3. During daytime and around sunset the flare-induced rΔNe at low altitudes needs less time to reach its peak than at higher altitudes, whereas around sunrise the situation is different—that is, the fastest response occurs at middle altitudes. The results in equinox show that rΔNe at 120, 160, 200, 240, and 280 km reaches its peak at TAFO $\approx$ 70, 45, 25, 50, and 60 min, respectively.
4. Around daytime and sunrise rΔTEC increases rapidly and reaches a peak at TAFO $\approx$ 18 min; however, around sunrise rΔTEC increases more slowly, with its peak at TAFO $\approx$ 60 min. There are two main factors that cause the difference between sunrise and sunset TEC behavior: at the time of flare onset, the SZA around sunrise is larger than that around sunset; the SZA around sunrise decreases gradually with time, whereas the SZA around sunset increases gradually with time.
5. The flare-induced rΔTEC shows a local time variation asymmetrical with respect to local midday, especially in equinox and winter, with a larger rΔTEC in the morning than in the afternoon due to the smaller background TEC in the morning. Whereas in summer, it occurs at about 12 LT.

Acknowledgements

The SEM/SOHO EUV data are downloaded from the web site: http://www.usc.edu/dept/space_science/semdatafolder/long/—The CELIAS/SEM experiment on the Solar Heliospheric Observatory (SOHO) spacecraft (SOHO is a joint European Space Agency, United States National Aeronautics and Space Administration mission). This research was supported by the National Natural Science Foundation of China (40674090, 40636032), the KIP Pilot Project (kzcx3-sw-144) of the Chinese Academy of Sciences, and the National Important Basic Research Project (2006CB806306). The National Center for Atmospheric Research (NCAR) is supported by the US National Science Foundation.

References

Afraimovich, E.L., 2000. GPS global detection of the ionospheric response to solar flares. Radio Science 35 (6), 1417–1424.

Chen, B., Liu, L., Wan, W., Ning, B., Ding, F., 2005. A statistical analysis of SITEC caused by intense solar flares during 1996–2003. Chinese Journal of Space Science 25 (1), 6–16.

Donnelly, R.F., 1967. The solar flare radiations responsible for sudden frequency deviations. Journal of Geophysical Research 72, 5247–5256.

Donnelly, R.F., 1969. Contribution of X-ray and EUV bursts of solar flares to sudden frequency deviations. Journal of Geophysical Research 74, 1873–1877.

Garriott, O.K., da Rosa, A.V., Davis, M.J., Villard Jr., D.G., 1967. Solar flare effects in the ionosphere. Journal of Geophysical Research 72, 6099–6103.

Garriott, O.K., da Rosa, A.V., Wagner, L.A., Thome, G.D., 1969. Enhancement of ionizing radiation during a solar flare. Solar Physics 8, 226–239.

Hargreaves, J.K., 1992. Effects of solar flares. In: Dessler, A.J., Houghton, J.T., Rycroft, M.J. (Eds.), The Solar–Terrestrial Environment. Cambridge University Press, Cambridge, UK, pp. 261–266.

Huba, J.D., Warren, H.P., Joyce, G., Pi, X., Iijima, B., Coker, C., 2005. Global response of the low-latitude to midlatitude ionosphere due to the Bastille Day flare. Geophysical Research Letters 32, L15103.

Lei, J., Liu, L., Wan, W., Zhang, S.-R., 2004a. Modeling the behavior of ionosphere above Millstone Hill during the September 21–27, 1998 storm. Journal of Atmospheric and Solar-Terrestrial Physics 66, 1093–1102.

Lei, J., Liu, L., Wan, W., Zhang, S.-R., 2004b. Model results for the ionospheric lower transition height over mid-latitude. Annales Geophysicae 22, 2037–2045.

Leonovich, L.A., Afraimovich, E.L., Romanova, E.B., Taschilin, A.V., 2002. Estimating the contribution from different ionospheric regions to the TEC response to the solar flares using data from the international GPS network. Annales Geophysicae 20, 1935–1941.

Liu, J.Y., Lin, C.H., Tsai, H.F., Liou, Y.A., 2004. Ionospheric solar flare effects monitored by the ground-based GPS receivers: theory and observation. Journal of Geophysical Research 109, A01307.

Mariska, J.T., Emslie, A.G., Li, P., 1989. Numerical simulations of impulsively heated solar flares. Astrophysical Journal 341, 1067.

Meier, R.R., et al., 2002. Ionospheric and dayglow responses to the radiative phase of the Bastille Day flare. Geophysical Research Letters 29 (10), 1461.

Mendillo, M., Evans, J.V., 1974. Incoherent scatter observations of the ionospheric response to a large solar flare. Radio Science 9, 197–210.

Picone, J.M., Hedin, A.E., Drob, D.P., Aikin, A.C., 2002. NRLMSISE-00 empirical model of the atmosphere: statistical comparisons and scientific issues. Journal of Geophysical Research 107 (A12), 1468.

Richards, P.G., Fennelly, J.A., Torr, D.G., 1994. EUVAC: a solar EUV flux model for aeronomic calculations. Journal of Geophysical Research 99, 8981–8992.

Richards, P.G., Woods, T.N., Peterson, W.K., 2006. HEUVAC: a new high resolution solar EUV proxy model. Advances in Space Research 37, 315–322.

Rishbeth, H., Garriott, O.K., 1969. Introduction to Ionospheric Physics. Academic Press, San Diego, CA.

Thome, G.D., Wagner, L.S., 1971. Electron density enhancement in the E and F regions of the ionosphere during solar flares. Journal of Geophysical Research 76, 6883–6894.

Titheridge, J.E., 1996. Direct allowance for the effect of photoelectrons in ionospheric modeling. Journal of Geophysical Research 101 (A1), 357–369.

Titheridge, J.E., 1997. Model results for the ionospheric E-region: solar and seasonal changes. Annales Geophysicae 15, 63–78.

Tsurutani, B.T., et al., 2005. The October 28, 2003 extreme EUV solar flare and resultant extreme ionospheric effects: comparison to other Halloween events and the Bastille Day event. Geophysical Research Letters 32, L03S09.

Wan, W., Liu, L., Yuan, H., Ning, B., Zhang, S., 2005. The GPS measured SITEC caused by the very intense solar flare on July 14, 2000. Advances in Space Research 36, 2465–2469.

Warren, H.P., Mariska, J.T., Lean, J., 1998. A new reference spectrum for the EUV irradiance of the quiet Sun 1. Emission measure formulation. Journal of Geophysical Research 103 (A6), 12077–12090.

Warren, H.P., Mariska, J.T., Lean, J., 2001. A new model of solar EUV irradiance variability: 1. Model formulation. Journal of Geophysical Research 106 (A8), 15745–15758.

Woods, T.N., Eparvier, F.G., 2006. Solar ultraviolet variability during the TIMED mission. Advances in Space Research 37 (2), 219–224.

Zhang, D.H., Xiao, Z., 2000. Study of the ionospheric TEC using GPS during the large solar flare burst on Nov. 6, 1997. Chinese Science Bulletin 45, 1749–1752.

Zhang, D.H., Xiao, Z., Igarashi, K., Ma, G.Y., 2002. GPS-derived ionospheric total electron content response to a solar flare that occurred on 14 July 2000. Radio Science 37 (5), 1086.

Zhang, D.H., Xiao, Z., 2005. Study of ionospheric response to the 4B flare on 28 October 2003 using international GPS service network data. Journal of Geophysical Research 110, A03307.